This is a repository copy of *Ion-exchange kinetics and thermal decomposition characteristics of Fe 2+-exchanged alginic acid membrane for the formation of iron oxide nanoparticles*.

White Rose Research Online URL for this paper:
http://eprints.whiterose.ac.uk/99446/

Version: Accepted Version

Ion-exchange kinetics and thermal decomposition characteristics of Fe²⁺-exchanged alginic acid membrane for the formation of iron oxide nanoparticles

Zihua Wang,[a] Jia Liu,[a] Girish M. Kale[a],* and Mojtaba Ghadiri[b]

[a]Institute for Materials Research, School of Process, Environmental and Materials Engineering, University of Leeds, Leeds LS2 9JT, U.K.

[b]Institute of Particle Science and Engineering, School of Process, Environmental and Materials Engineering, University of Leeds, Leeds LS2 9JT, U.K.

*Author for all correspondences: g.m.kale@leeds.ac.uk (E); 0044-113-3432805 (T)

Abstract

The ion-exchange kinetics of Fe^{2+} cations in aqueous solution with H^+ from alginic acid have been analyzed in this study as a function of contact time lengths using Inductively Coupled Plasma - Atomic Emission Spectrometry analysis (ICP-AES). The kinetic parameters have been evaluated using pseudo 1st or 2nd order models and a consistent ion-exchange mechanism is suggested. Furthermore, an insight into the calcination of Fe^{2+} ion-exchanged alginic acid process has been obtained by using simultaneous Thermo-Gravimetric Analysis and Differential Scanning Calorimetry (TGA/DSC) and High Temperature X-ray diffraction (HT-XRD).

Keywords: Alginic acid membrane, Ion-exchange kinetics, Thermo-gravimetric analysis, Differential scanning calorimetry, high temperature XRD

1. Introduction

Sodium alginate (Na-ALG, $NaC_6H_7O_6$) is a polymer extracted from brown seaweed. It contains varying amount of 1, 4´-linked β-D-mannuronic acid (M) and α-L-guluronic acid (G) residues. Gelation of alginate is due to the interaction of carboxylate groups with metal ions [1] in aqueous solution. Most of the research in understanding sodium alginate mediated ion-exchange process in related to pharmaceutical science and food chemistry [2-5]. Not much has been done to understand this phenomenon with respect to the production of high surface area ceramic oxide particles until recently [6, 7]. It has been discovered that, during gelation and subsequent calcinations of the metal alginate gels, the ions become immobile and cannot readily come closer to each other, hence providing an excellent basis for producing small metal oxide particles [6, 7] in nano to micrometer size range.

Hematite (α-Fe_2O_3) is the most stable phase form of iron oxide under ambient conditions. It is widely used in solar cells to increase the photo-conversion efficiency [8], lithium ion battery to improve the lithium intercalation performance [9], gas sensors due to the differences in electrical resistivity in oxidizing/reducing gases [10], photo-catalysts under visible-light irradiation [11], field emission devices due to the high emission current density [12], field effect transistors when hematite is doped with zinc to achieve p- or enhance n-type semiconducting property [13] and as photo-catalyst for photon emitted water splitting [14] due to its low cost and high resistance to corrosion.

Although metal alginate gels obtained by dropping sodium alginate solution into different aqueous solution to form beads have been used for various applications, the kinetics of ion-exchange process itself has not been studied in details because the gelation time is rapid and the amount of metal ion exchanged in each alginate bead is too small to be detected. In this article,

the investigation of ion-exchange kinetics between proton exchanged sodium alginate beads and ferrous ions in an aqueous solution is presented. Additionally the result of the synthesis of α-Fe_2O_3 by thermal decomposition of iron alginate gels is also presented. The rate of cation exchange process is characterized by Inductively Coupled Plasma - Atomic Emission Spectrometry analysis (ICP-AES), whereas the Fe_3O_4/Fe_2O_3 transformation has been characterized by simultaneous Thermo-Gravimetric Analysis and Differential Scanning Calorimetry (TGA/DSC) and High Temperature X-ray diffraction (HT-XRD). Details of the experimental process and research findings are described below.

2. Experimental procedure

Commercial sodium alginate powders were purchased from Fisher Scientific Ltd, UK. Ferrous chloride tetra-hydrate $FeCl_2 \cdot 4H_2O$ (198.8 g mol^{-1}, technical purity) was purchased from MP Biomedicals Europe, France. Sodium alginate solution at a concentration of 4 wt% was prepared by dissolving an appropriate amount of sodium alginate in distilled water while stirring, denoted as Solution 1. Alginic acid (H-ALG, $HC_6H_7O_6$) beads were prepared by dripping Solution 1 through a 16 G (1.194 mm) inner diameter stainless steel needle attached to a 20 mL syringe into 200 mL hydrochloric acid (1 M) denoted as Solution 2. The gelatinous beads of alginate were maintained in HCl Solution 2 for 20 min under gentle magnetic stirring for facilitating the ion-exchange reaction between Na^+ and H^+. The H-ALG beads were then removed from the solution by sieving through a stainless steel sieve and were subsequently washed with distilled water and further reacted with Metal Solution 3. The metal solution was prepared from ferrous chloride by dissolving an appropriate amount of the respective salts in distilled water at ambient temperature. The cationic concentration of Metal Solution 3 was controlled at 0.1 M. The beads were respectively kept in Metal Solution 3 for 1, 3, 5, 7, 10 and 20 min under gentle magnetic stirring

for promoting the ion-exchange reaction between H^+ and Fe^{2+}. After separated from the solution through stainless steel sieves, these Fe^{2+} ion-exchanged beads were further washed with distilled water and dried in a convection oven for 24 hours at 90 °C until they were completely dried.

The kinetics of ion-exchange process in the present study was investigated in metal-ion rich solutions where the initial concentration of $[Fe^{2+}]_0 \gg [Na^+ / H^+]_0$. The volume ratio in this study was maintained constant with Na-ALG:H-ALG:Fe-ALG = 1:1:1. The kinetic studies were based on charactering the reduction of the metal ion concentration in the remaining solution as a function of time. For this purpose, after separating by sieving the Fe-ALG beads from the ionic solution, the filtrate solutions after ion-exchange for different time lengths was diluted 100,000 times with deionized water and the concentration of Fe^{2+} in the electrolyte was determined by employing ICP-AES technique. Moreover, the phase evolution of the dried beads sample (after 20 min reaction time) was also investigated by simultaneous TGA/DSC analysis (Mettler Toledo STAR^e System, Leicester, UK) in controlled atmosphere of air at a flow rate of 50 mL min^{-1} from ambient temperature up to 1000 °C with the heating rate maintained at 3 °C min^{-1} without any holding time. The mass of the sample used in the TGA/DSC experiment was 15 mg. These Fe-ALG dried beads were placed on a platinum substrate and analyzed using HT-XRD (Anton Paar HTK-1200, Almelo, The Netherlands) employing Cu Kα radiation. The heating program was set to increase the temperature in 25 °C intervals from room temperature to 1000 °C with the heating rate maintained at 3 °C min^{-1} in static air condition. At each temperature, 30 min dwell time was allowed in order to complete the thermal reaction and allow the sample to attain thermal equilibrium condition. HT-XRD scan was performed over a range $2\theta = 20°\text{-}70°$ using a step size of ca. 0.033°.

3. Results and Discussion

The stoichiometry of ion exchange requires that the fluxes of the two exchanging counter ions be equal in magnitude, even though the counter ion mobility may be quite different between each other [15, 16]. Therefore, any H^+ ion leaving the alginic acid beads must be replaced by an equivalent amount of Fe^{2+} metal ions.

The kinetics of ion-exchange process in the present study was investigated in metal-ion rich solutions, where the initial concentration of $[Fe^{2+}]_0$ was much greater than that of $[H^+]_0$. The residual Fe^{2+} metal ion concentration in the solution was measured periodically until it reached an asymptotic value, indicating the attainment of steady-state condition in the ion-exchange reaction. The stoichiometry of this gelation process can be expressed by the following exchange reaction:

$$2n(H - ALG) + x \cdot Fe^{2+} = n(Fe - ALG) + 2x \cdot H^+ \tag{1}$$
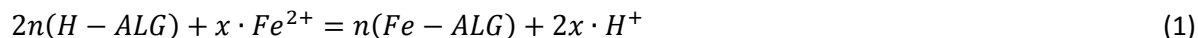
The experimental data of the variation of Fe^{2+} concentration in alginate beads as a function of time is shown in Figure 1, where a relatively fast ion-exchange in observed. It can be clearly seen in Figure 1 that the initial rate of ion exchange is significantly rapid which progressively reaches an equilibrium value at 10 min. This can be explained on the basis that when the Fe^{2+} metal ions come in contact with the alginic acid beads, a rapidly inward ion-exchange take place and the H^+ ions from the inner core of alginic acid beads begin to diffuse outward into the Fe^{2+} electrolyte solution through the converted shell layer, and simultaneously, the metal Fe^{2+} ions diffuse inward to maintain charge neutrality. The process is therefore a counter current transfer of ions leading to a growth of converted shell. Based on the initial rate of uptake of Fe^{2+}, it can be concluded that the kinetic of the ion-exchange is in fact very fast and the mass transfer is controlled by the ion diffusion through the converted layer. The internal structure of the polymer

gel is likely to be significantly open as seen in our early study of porous freeze dried ion-exchanged alginate beads using X-ray tomography [16]. Nevertheless the water in the structure is stationary and hence provides a required continuous medium for the Fe^{2+} ions to diffuse through it to reach to H^+ in the inner core.

An appropriate kinetic model is needed to describe the mass transfer process in this system. Homogeneous surface diffusion, pore diffusion and heterogeneous diffusion models have been proposed in the literature however owing to their complexity they are of limited practical utility value [17]. Therefore, a simplified kinetic model has been used to analyze the chronographic data obtained in this study. The chronographic data have been fitted to the first order model [18] and second order model [19] using Origin 8.0 software. The expression of first order kinetic model [18] is given by the following equation:

$$\frac{dq_t}{dt} = k_1(q_e - q_t) \tag{2}$$

which on rearranging gives,

$$q_t = q_e[1 - \exp(-k_1 t)] \tag{3}$$

where q_t is the ion concentration in the solution at time t; q_e denotes asymptotic value and k_1 is the first order rate constant and t is the time of reaction in seconds.

The second order kinetic model [19] is expressed as follows:

$$\frac{1}{(q_e - q_t)} = \frac{1}{q_e} + k_2 t \tag{4}$$

Rearranging the above expression gives,

$$\frac{t}{q_t} = \frac{1}{k_2 q_e^2} + \frac{t}{q_e} \tag{5}$$

$$\frac{t}{q_t} = \frac{1}{h} + \frac{t}{q_e} \tag{6}$$

where $h = k_2 q_e^2$ and k_2 is the second order rate constant.
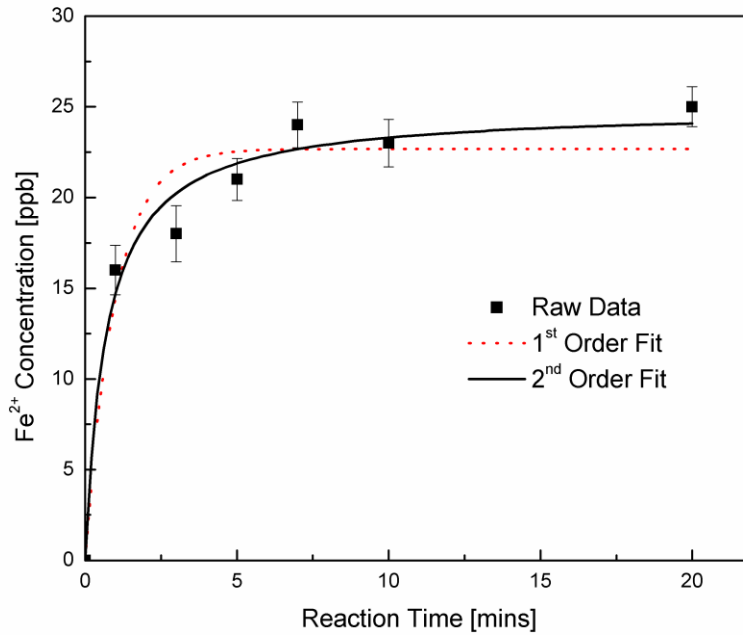
Fig. 1 1st-order vs. 2nd-order fit for the Fe^{2+} ion-exchange reaction between aqueous phase and alginate gel beads as a function of contact time. Dotted line and solid line show the 1st order and 2nd order fit to the data, respectively.

It can be clearly seen from Figure 1 that the data fits better with the second order kinetic model than the first order. The first order model fits the experimental data well in the initial fast ion exchange stage with reaction times less than 2 min. However, the fitted curve deviates from the obtained data at t > 2 min, whereas, the second order model fits the entire experimental data considerably better.

Table 1 Parameters of Diffusion Models.

Pseudo-1st-order	Value	SD	Pseudo-2nd-order	Value	SD
q_e	22.67	1.09	q_e	24.92	1.06
k_1	1.02	0.28	k_2	0.06	0.01
r^2	0.93		r^2	0.97	
Reduced Chi-Sqr	4.99		Reduced Chi-Sqr	2.03	

As shown in Table 1, the r^2 value obtained from second order is 0.97 which is higher than 0.93 obtained from first order model. The reduced chi square value obtained using 2nd-order is lower than the 1st-order. This indicates that the second order model can be better applied to this ion exchange process.
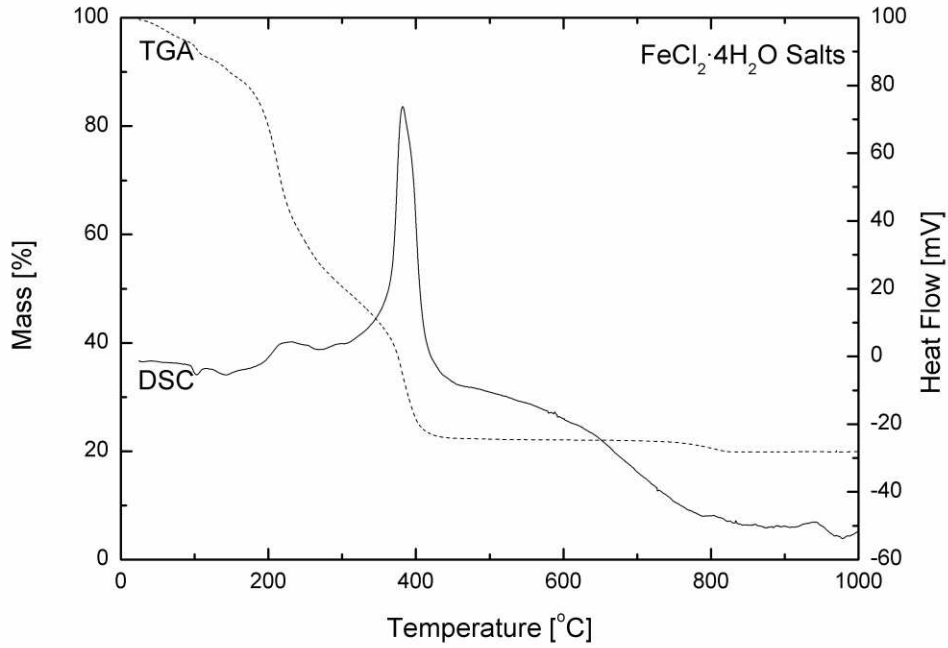
Fig. 2 Thermal analysis of Fe-ALG dried beads.

The progress of calcination of dried ion-exchanged Fe-ALG beads (after 20 min reaction) was studied by simultaneous TGA/DSC and HT-XRD, respectively. Four decomposition processes were observed (see Figure 2) in the temperature range of ambient ~ 200 °C, 200-275 °C, 350-420 °C and 700-900 °C, respectively. An endothermic decomposition peak was observed at temperatures between ambient and 200 °C, corresponding to about 10% weight loss as shown in the TGA profile. This was possibly due the evaporation of water during heat treatment. At temperature between 200-275 °C, about 30% weight loss was observed in the TGA profile. This is probably due to the cleavage of weaker linkages between β-D-mannuronic acid (M) and α-L-guluronic acid (G) residues in the alginate polysaccharide molecule leading to significant evolution of oxygen. This is believed to simultaneously promote the oxidation of Fe^{2+} ions chelated in alginate structure to form coexisting Fe_2O_3 as seen in Figure 3. The net result of the above two simultaneous endothermic and exothermic processes led to the formation of a net mildly exothermic peak as seen in the DSC trace of Figure 2. The β-D-mannuronic acid (M) and α-L-guluronic acid (G) residues in the alginate structure were finally completely oxidized leading to a further 20% weight loss at higher temperature between 350-420 °C with a corresponding large exothermic peak in the DSC profile. It is possible that during this decomposition process, there is perhaps a lack of availability of oxygen that leads to the formation of co-existing Fe_3O_4 and Fe_2O_3 oxide mixture (see Figure 3). Furthermore, in the temperature range from 700 to 900°C, another endothermic peak was observed with about 3% weight loss in the TGA profile. This may be due to the partial reduction of stoichiometric Fe_2O_3 to an oxygen deficient Fe_2O_{3-x} phase at high temperature with an estimatical value of x = 0.03.
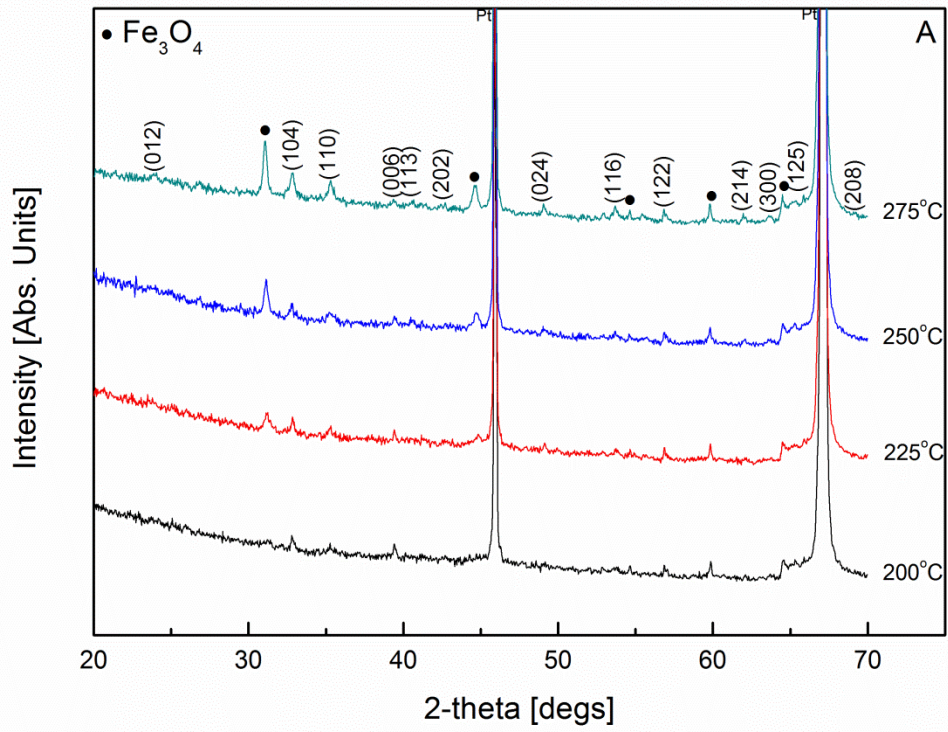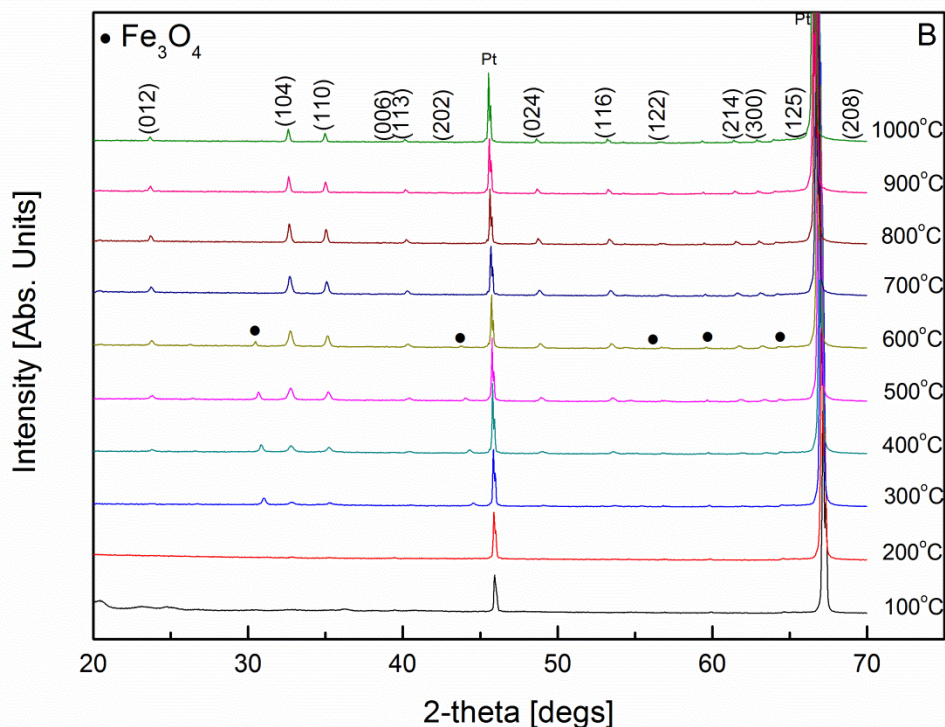
Fig. 3 HT-XRD of Fe-ALG dried beads **A** between 200 and 275 °C and **B** between 100 and 1000 °C, respectively. The patterns are indexed by ICDD 00-033-0664 as rhombohedral Fe_2O_3 shown at the top of the peaks. Tick marks "•" for reference pattern of Fe_3O_4 (ICDD 00-026-1136) and tick marks "Pt" for reference pattern of Pt (ICDD 00-004-0802) are shown at the top of the respective peaks.

HT-XRD was performed in static air condition on a Pt substrate and the results are shown in Figure 3A and 3B. Clean, single phase rhombohedral α-Fe_2O_3 HT-XRD pattern was observed at temperature range between 700 and 1000 °C which agreed with the TGA/DSC analysis shown in Figure 2. It should be noted that the temperature shift observed for various reaction steps between TGA/DSC, and HT-XRD was because of the dynamic nature of TGA/DSC experiments compared with the static HT-XRD experiments.

No XRD peaks (apart from Pt substrate) were observed in Figure 3A at temperatures below 200 °C indicating that Fe-ALG dried beads did not fully crystallize below 200 °C. The signature of amorphous nature of the Fe-ALG beads is evident from the drift of the baseline at low angle up to 300 °C which progressively becomes less dominant as temperature increases from 200 °C to 300 °C. Furthermore, HT-XRD pattern indicated that Fe_3O_4 magnetite (ICDD 00-026-1136) and Fe_2O_3 (ICDD 00-033-0664) phases were both coexistent at 200 °C as seen in Figure 3A. This was due to the initial decomposition of Fe-ALG resulting from the cleavage of carbon bonds between Fe^{2+} metal ions and carboxylate groups in alginate structure followed by the gradual oxidation of Fe^{2+} incorporated in the alginate structure from $FeCl_2$ solution during the ion exchange process to Fe^{3+} with increase in temperature from 200 to 600 °C. As expected, initially the formation of Fe_3O_4 dominated over Fe_2O_3 with increasing temperature from 200 to 400 °C. Increasing the temperature further from 400 to 625 °C, the peak intensity of Fe_3O_4 magnetite gradually reduced, indicating the progressive conversion of Fe_3O_4 into Fe_2O_3 rhombohedral phase in air as shown in Figure 3B. At 650 °C and above no traces of Fe_3O_4 were seen in the X-ray diffraction patterns indicating that Fe_3O_4 converted entirely into Fe_2O_3.

Previous research [20] has shown that the profile broadening in diffraction data is influenced by a number of factors, such as instrument broadening, coherence length, micro-strain, compositional homogeneity or a combination thereof. For nanopowders, particle size effects show a far better description of the XRD broadening in comparison to the micro-strain [6, 7, 16]. Therefore, the particle sizes of Fe_3O_4 and Fe_2O_3 nanopowders at 225 °C were calculated using Scherrer equation as shown below.

$$\tau = \frac{K\lambda}{\beta cos\theta} \qquad (7)$$

where τ is the mean crystallite size, K is a shape factor, λ is the X-ray wavelength, β is the line broadening at half the maximum intensity (FWHM) and θ is the Bragg angle, respectively. The crystallite size is about 38 and 42 nm for Fe_3O_4 and Fe_2O_3 based on the (220) and (104) plane at 225 °C, respectively. The crystallite size of the obtained sample was found to increase with increase in temperature, which resulted in the increase in peak intensity and reduction in the peak broadening.

4. Conclusions

In this communication, the kinetics of ion-exchange reaction is studied using alginic acid (H-ALG) in a relatively simple condition and described numerically by 1st and 2nd order models. The low value of reduced chi square obtained using second order model indicates that the 2nd-order model is more applicable to this type of ion exchange process. The TGA/DSC results indicate that thermal decomposition process is complete at about 450 °C which leads to a formation of single phase α-Fe_2O_3. The HT-XRD data also lends support to this conclusion. In this sol-gel production method, the homogeneous distribution of metal ions in the polymer structure and slow collapse of the carbohydrate structure during calcination prevent the rapid agglomeration of metal ions, which ensures small particle size of the product and high purity single phase material is formed at low temperature.

Acknowledgement

References

1. Gombotz WR, Wee SF (1998) Protein release from alginate matrices. Adv Drug Deliver Res 31: 267-285

2. Wu J, Kong T, Yeung KWK, Shum HC, Cheung KMC, Wang L, To MKT (2013) Fabrication and characterization of monodisperse PLGA-alginate core-shell microspheres with monodisperse size and homogeneous shells for controlled drug release. Acta Biomater 9: 7410-7419

3. Moshaverinia A, Ansari S, Chen C, Xu X, Akiyama K, Snead ML, Zadeh HH, Shi S (2013) Co-encapsulation of anti-BMP2 monoclonal antibody and mesenchymal stem cells in alginate microspheres for bone tissue engineering. Biomaterials 34: 6572-6579

4. Jiang T, Feng L, Wang Y (2013) Effect of alginate/nano-Ag coating on microbial and physicochemical characteristics of shiitake mushroom (Lentinus edodes) during cold storage. Food Chem 141: 954-960

5. Vu CHT, Won K (2013) Novel water-resistant UV-activated oxygen indicator for intelligent food packaging. Food Chem 140: 52-56

6. Wang ZH, Kale GM, Ghadiri M (2011) Novel Ion-exchange process for the preparation of Metal Oxide nanopowders from Sodium Alginate. J Am Ceram Soc 95: 3124-3129

7. Wang ZH, Kale GM, Ghadiri M (2012) Alginate mediated novel ion-exchange process for the production of $Ce_xGd_{1-x}O_{2-\delta}$ nanopowders. Chem Eng J 198-199: 149-153

8. Beermann N, Vayssieres L, Lindquist SE, Hagfeldt A (2000) Photoelectrochemical Studies of Oriented Nanorod Thin Films of Hematite. J Electrochem Soc 147: 2456-2461

9. Zeng SY, Tang KB, Li TW, Liang ZH, Wang D, Wang YK, Qi YX, Zhou WW (2008) Facile Route for the Fabrication of Porous Hematite Nanoflowers: Its Synthesis, Growth Mechanism, Application in the Lithium Ion Battery, and Magnetic and Photocatalytic Properties. J Phys Chem C 112: 4836-4843

10. Chauhan P, Annapoorni S, Trikha SK (1999) Humidity-sensing properties of nanocrystalline haematite thin films prepared by sol-gel processing. Thin Solid Films 346: 266-268

11. Frank SN, Bard AJ (1977) Heterogeneous photocatalytic oxidation of cyanide and sulfite in aqueous solutions at semiconductor powders. J Phys Chem 81: 1484-1488

12. Yu T, Zhu YW, Xu XJ, Yeong KS, Shen ZX, Chen P, Lim CT, Thong JT, Sow CH (2006) Substrate-Friendly Synthesis of Metal Oxide Nanostructures Using a Hotplate. Small 2: 80-84

13. Fan ZY, Wen XG, Yang SH, Lu JG (2005) Controlled p- and n-type doping of Fe_2O_3 nanobelt field effect transistors. Appl Phys Lett 87: 013113

14. Chernomordik BD, Russell HB, Cvelbar U, Jasinski JB, Kumar V, Deutsch T, Sunkara MK (2012) Photoelectrochemical activity of as-grown, $\alpha-Fe_2O_3$ nanowire array electrodes for water splitting. Nanotechnology 23: 194009

15. Khairou KS, Al-Gethami WM, Hassan RM (2002) Kinetics and mechanism of sol‒gel transformation between sodium alginate polyelectrolyte and some heavy divalent metal

ions with formation of capillary structure polymembranes ionotropic gels. J Membrane Sci 209: 445-456

16. Wang ZH, Kale GM, Yuan QC, Ghadiri M (2012) X-Ray micro-tomography of freeze dried nickel alginate beads and transformation into NiO nanopowders. RCS Advances 2: 9993-9997

17. Cheung C, Porter JF, McKay G (2001) Sorption kinetic analysis for the removal of cadmium ions from effluents using bone char. Water Res 35: 605-612

18. Lagergren S (1898) Zur theorie der sogenannten adsorption gelöster stoffe. Kungliga Svenska Vetenskapsakademiens. Handlingar 24: 1-39

19. Ho YS, McKay G (1999) Pseudo-second order model for sorption processes. Process Biochem 34: 451-465

20. Wang ZH, Comyn TP, Ghadiri M, Kale GM (2011) Maltose and pectin assisted sol–gel production of $Ce_{0.8}Gd_{0.2}O_{1.9}$ solid electrolyte nanopowders for solid oxide fuel cells. J Mater Chem 21: 16494-16499